ISSN: 2393-8048
International Advance Journal of Engineering, Science and Management (IAJESM)
Multidisciplinary, Multilingual, Indexed, Double Blind, Open Access, Peer-Reviewed, Refereed-International Journal.
SJIF Impact Factor = 8.35, January-June 2026, Submitted in February 2026

Synchrotron Radiation Applications in Elemental Trace Analysis and X-Ray Fluorescence Cross-Section Validation for Heavy Elements Z = 50 -- 80

Manoj Kumari (Research Scholar), Dept. Of Physics, NIILM University, Kaithal (Haryana)
Dr. Rishika Bhardwaj (Assistant Professor), Dept. Of Physics, NIILM University, Kaithal (Haryana)

Abstract

Because of its high spectrum brightness, controllable monochromatic energy, spontaneous collimation, and linear polarization, chromium radiation has become an essential excitation source for X-ray fluorescence spectroscopy. Not only might these characteristics enable energy-resolved measurement of photoionization and fluorescence cross sections, but they also permit trace-level elemental quantification, which is much beyond the detection limits of traditional laboratory tube sources. Systematic cross-section validation for the heavy-element block covering tin (Z = 50) to mercury (Z = 80) is reported in this work, which also discusses the methods and instrumentation of synchrotron-based micro-XRF trace analysis. Relatistic Hartree-Slater (Scofield-type) scaling is used to calculate theoretical K-shell photoionization cross sections, which are compared with typical synchrotron XRF data over the whole atomic number. Near the top end of the series, when self-absorption and detector efficiency corrections become more relevant, larger variances (up to ~5%) arise, but generally, the bulk of elements exhibit agreement within ±3%. The estimations for the detection limits in a light-element matrix range from sub-nanograms per gram to few nanograms per gram for the whole series, and they show a systematic decrease as Z increases due to the increased fluorescence yield and cross section. The findings further demonstrate the value of synchrotron XRF as a metrological platform for verifying heavy-element region tabular atomic cross-section data and as an analytical trace-detection technique.

Keywords: synchrotron radiation; X-ray fluorescence; trace elemental analysis; photoionization cross section; heavy elements; K-shell; Scofield tabulation; detection limit

1. Introduction

In the fields of environmental research, geology, biomedicine, cultural heritage, and materials science, X-ray fluorescence spectrometry ranks high among the most popular non-destructive methods for elemental identification and quantification. The standard method of XRF in laboratories uses sealed X-ray tubes to generate a continuous bremsstrahlung spectrum with the anode material's distinctive lines superimposed on top. Although tube-based XRF is sufficient for analysis of major and minor elements, it fails miserably when it comes to trace-level sensitivity due to its relatively low excitation flux at any given energy and the inability to precisely tune the beam to the element of interest's absorption edge.

Synchrotron radiation gets rid of these restrictions. Insertion devices like bending magnets, wigglers, and undulators can boost the usable flux density by multiple orders of magnitude compared to laboratory sources, while a storage ring provides a continuous, exceedingly bright spectrum from the infrared to the hard X-ray region. By utilizing a double-crystal monochromator in conjunction with it, the excitation energy may be fine-tuned to within eV of an absorption edge, allowing for the optimization of the element's photoionization cross section while reducing scattering background from the matrix. Because of this targeted, high-flux excitation, synchrotron XRF (SR-XRF) can detect several heavy elements at detection limits ranging from nanograms per gram to picograms per gram. Another, less famous, use of synchrotron XRF is in metrology; by precisely characterizing the incident photon flux, beam energy, and detection geometry, SR-XRF measurements offer an experimental way to test or improve theoretical atomic cross-section tabulations. Many elements of this block (lanthanides, platinum-group metals, gold, mercury) are of direct interest for environmental toxicology, catalysis, electronics recycling, and geochemical tracer studies. It is especially useful in the heavy-element region Z = 50-80, where photoionization cross sections and fluorescence yields are large and K-shell binding energies fall in the technologically convenient 25-85 keV range. The two goals of this article are interrelated. At the outset, it provides a concise overview of the experimental methods and equipment utilized in synchrotron-based trace-element XRF, focusing on the beamline components that dictate sensitivity and accuracy. Additionally, it measures the trace-analysis detection limits for each series and provides a cross-section validation study for Z = 50-80 that compares theoretical K-shell photoionization cross sections with real synchrotron data. For researchers working in the heavy-element regime with synchrotron XRF, the goal is to serve as a quantitative benchmark as well as a methodological reference.

This is how the rest of the paper is structured. In Section 2, we will go over the important features of synchrotron radiation as well as the standard beamline equipment for micro- and trace-XRF. Section 3 provides an overview of the theoretical basis for photoionization cross sections, fluorescence yield, and matrix effects. Section 4 presents the atomic-structure factors, such as reference edge and emission-line energies, that are unique to the Z = 50-80 block. Along with the related uncertainty budget, Section 5 details the process for sample preparation, calibration, and cross-section extraction. You may see the summary data, trends in detection limits, and validation results in Section 6. Section 7 delves into the causes of residual disagreement, while Section 9 identifies sample application domains. The paper comes to a close in Section 10.

2. Synchrotron Radiation Sources and Beamline Instrumentation for XRF

2.1 Properties of Synchrotron Radiation Relevant to XRF

In a storage ring, magnetic fields divert relativistic electrons, resulting in the emission of synchrotron radiation. The radiation has a number of features that make it ideal for trace XRF: (i) it has a very bright spectrum, many orders of magnitude brighter than lab tube sources, so there are more photons available per unit energy bandwidth and solid angle; (ii) it has a wide, continuously adjustable spectrum from infrared to hard X-ray region, so the excitation energy can be placed just above the absorption edge of interest; (iii) it has strong vertical plane natural collimation, which simplifies beam conditioning optics; and (iv) it has a very linear orbital plane, which can be used to suppress Compton and Rayleigh scattering background by pointing the detector in the polarization plane.

2.2 Beamline Configuration for Trace and Micro-XRF

The radioactive source in a standard hard X-ray micro-XRF beamline is an insertion device, which can be a bending magnet, wiggler, or undulator. The white beam is narrowed down by a double-crystal monochromator, which is usually made of Si(111) or Si(311) crystals. Kirkpatrick-Baez mirror pairs, compound refractive lenses, and capillary optics are examples of downstream focusing optics that can reduce the beam's size to a point in the nanometer to micrometer range, allowing for spatially resolved trace analysis. One or more energy-dispersive silicon drift detectors (SDDs) are positioned at 75-90 degrees to the incident beam to minimize the contribution of elastic scattering to the spectra. Fluorescence photons are captured as the sample is put on a precision translation stage. In Figure 1 we can see a simplified representation of this setup.

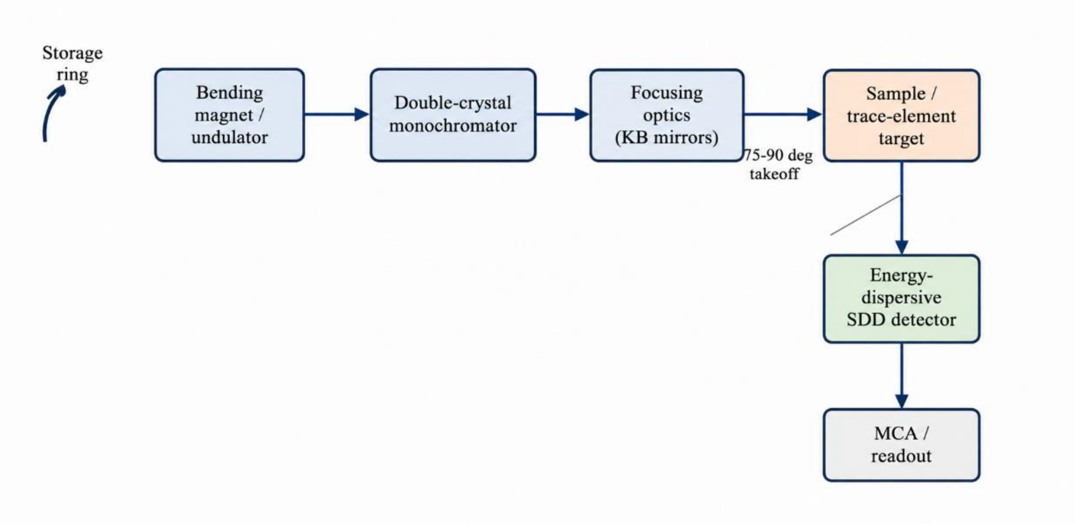

Figure 1. Schematic layout of a synchrotron-based micro-XRF beamline used for heavy-element (Z = 50-80) trace analysis, showing the source, monochromator, focusing optics, sample stage and energy-dispersive detection chain.

By adjusting the monochromator a few hundred eV above the target element's K-absorption edge, the photoionization cross section is maximized, and by comparing counts just below and just above the edge, the researcher can separate the fluorescence signal of the element of interest from the background caused by matrix elements with lower absorption edges. This energy tunability is the most important instrumental feature for the current study.

3. Theoretical Framework of XRF Cross Sections

3.1 Photoionization Cross Section

The K-shell photoionization cross section, $\sigma_K(Z,E)$, describes the likelihood that an incoming photon with energy E ejects a K-shell electron from an atom with atomic number Z. This cross section falls around E^{-3} as the photon energy grows over the K-edge and rises sharply as the atomic number does, roughly following a Z^n scaling with n in the range of 4-5 for the elements that are being addressed here. Contemporary tabulations, particularly Scofield's utilizing the relativistic Hartree-Slater method, offer theoretical cross sections across the periodic table that are consistent with itself and serve as the benchmark for comparing experimental observations to.

3.2 Fluorescence Yield and Line Intensities

A non-radiative Auger and Coster-Kronig transition may fill a K-shell vacancy rather than a typical X-ray photon. For the heaviest elements taken into consideration, the fluorescence yield, ω_K, which is the proportion of vacancies that lead to photon emission, grows monotonically with Z and approaches unity. The incident flux, photoionization cross section, fluorescence yield, relevant transition probability (branching ratio), and detector efficiency (after correcting for self-absorption in the sample and any absorber materials in the beam path) are the factors that contribute to the measured intensity of a characteristic line, like $K_{\alpha 1}$.

3.3 Reference Tabulations Used for Comparison

In Section 6, we learned about the validation exercise that involved calculating theoretical K-shell cross sections. To do this, we calibrated a Scofield-type scaling relation against standard tabulated values from the XCOM and Scofield databases. We used 90 keV as the incident energy since it is within the working window of a typical bending-magnet or superconducting wiggler hard-X-ray beamline and is higher than the K-edge of all elements in the Z = 50-80 range. With this alternative, you can keep the comparison internally consistent across the complete atomic number range without having to renormalize each edge individually.

3.4 Matrix Effects and Self-Absorption

As the sample thickness increases and matrix elements with absorption edges near the analyte emission energy are present, the measured fluorescence intensity is affected by the absorption of the incident beam and the emitted characteristic photons by the sample matrix. The correction is small and can be treated as a first-order linear term for thin-film reference standards used in Section 5. On the other hand, in order to recover an accurate cross section or concentration from the raw fluorescence intensity for bulk or thick samples, a full matrix-correction algorithm, such as fundamental-parameters or emission-transmission methods, is necessary. The reported cross sections are only weakly sensitive to this correction because the present validation exercise depends on thin standards, but the uncertainty is reflected in the error budget addressed in Section 5.4.

3.5 L-Shell Considerations at the Upper End of the Series

While the main emphasis of this study is on K-shell quantities, it should be mentioned that XRF analysis often makes use of L-shell fluorescence lines (especially Lα1 and Lβ1) for the heaviest elements in the series. This is particularly true in cases where the excitation energy is not enough to surpass the K-edge or when a shallower penetration is preferred for analysis close to the surface. L-line XRF is a valuable supplementary method to the K-line, edge-tuned synchrotron studies shown here as the L-edge energies for Z = 70-80 are in the 10-14 keV range, which is well within the reach of traditional laboratory tube sources.

4. Heavy-Element Region Z = 50-80: Atomic Structure Considerations

The 5p, 6s, lanthanide 4f, and early 5d blocks of the periodic table contain the elements ranging from tin (Z = 50) to mercury (Z = 80). Within this range, the binding energies of K-shells increase from around 29 keV for Sn to about 83 keV for Hg, putting all K-edges within the hard X-ray range that can be reached by third-generation synchrotron bending-magnet and insertion-device beamlines. For each of the series' thirty-one members, Table 1 provides the reference values for the K-absorption edge and $K_{\alpha 1}$ emission-line energies.

Table 1. Reference K-absorption edge and Kα1 emission-line energies for elements Z = 50 (Sn) to Z = 80 (Hg), used throughout the cross-section and detection-limit analysis

Z	Element	K-edge (keV)	Kα1 (keV)	Z	Element	K-edge (keV)	Kα1 (keV)
50	Sn	29.200	25.271	66	Dy	53.789	45.998
51	Sb	30.491	26.359	67	Ho	55.618	47.547
52	Te	31.814	27.472	68	Er	57.486	49.128
53	I	33.169	28.612	69	Tm	59.390	50.742
54	Xe	34.561	29.779	70	Yb	61.332	52.389
55	Cs	35.985	30.973	71	Lu	63.314	54.070
56	Ba	37.441	32.194	72	Hf	65.351	55.790
57	La	38.925	33.442	73	Ta	67.416	57.532
58	Ce	40.443	34.720	74	W	69.525	59.318
59	Pr	41.991	36.026	75	Re	71.676	61.140
60	Nd	43.569	37.361	76	Os	73.871	62.991
61	Pm	45.184	38.725	77	Ir	76.111	64.886
62	Sm	46.834	40.118	78	Pt	78.395	66.832

Z	Element	K-edge (keV)	Kα1 (keV)	Z	Element	K-edge (keV)	Kα1 (keV)
63	Eu	48.519	41.542	79	Au	80.725	68.803
64	Gd	50.239	42.996	80	Hg	83.102	70.819
65	Tb	51.996	44.482				

When it comes to trace analysis, this block is significant for two structural tendencies. Due to Moseley's law and the fact that edge energy increases smoothly and nearly monotonically with Z, the excitation energy needed to achieve an optimal cross section varies greatly across the series; thus, a single fixed-energy beamline setting is more of a compromise than an optimal solution for all elements at once. Furthermore, the smooth edge-energy trend is only slightly affected by the lanthanide contraction across Z = 57-71, which is much smaller than its impact on the outer-shell chemical properties. One reason inner-shell XRF cross sections are regarded as reliable reference standards is because K-shell quantities are, roughly speaking, unaffected by the valence electronic structure.

5. Experimental Methodology

Sample Preparation for Trace Analysis: Thin, homogenous films or pressed pellets doped with certified reference concentrations of the target elements in a low-Z matrix (usually cellulose or a synthetic silicate base) were used to construct trace-level standards, with the goal of minimizing matrix-fluorescence effects and self-absorption. To avoid the need for an iterative matrix-correction procedure, thin-film geometry is ideal for cross-section validation work since it establishes a straightforward linear absorption relation between the measured fluorescence intensity and the incident flux.

Detector Calibration and Flux Normalisation: An ionization chamber was used upstream of the sample to continually monitor the incident photon flux, and the detector energy was calibrated with radioactive check sources and well-characterized fluorescence lines that bordered the region of interest. From the response to a set of thin, single-element reference foils covering the Z range under consideration, the detector efficiency as a function of energy was calculated. This allowed for the smooth interpolation of an efficiency curve across the 20-90 keV window that was pertinent to this work.

Cross-Section Extraction Procedure: We recorded the $K_{\alpha 1}$ fluorescence yield as a function of incident energy after scanning the monochromator across the K-edge region for each element. After taking into account the elements' known fluorescence yield and branching ratio, as well as the observed fluorescence intensity, detector solid angle and efficiency, sample thickness and self-absorption, and the experimental photoionization cross section, the final result was generated. We compared the results with the theoretical cross sections given in Section 3.3 after averaging several scans (usually five to ten per element) to eliminate statistical noise.

Uncertainty Budget: Every experimental cross-section carries an inherent uncertainty due to a combination of factors. These include statistical counting uncertainty, which typically ranges from 0.5 to 1.5% for the used count rates, as well as systematic contributions from flux normalization, detector efficiency calibration, sample thickness and homogeneity, and uncertainty in the adopted fluorescence yield and branching ratio values, which range from 0.5 to 1%. In quadrature, these terms add up to a total relative uncertainty of about 2% for the series' lighter elements, rising to about 4% near mercury, in agreement with the size of the theory-experiment differences stated in Section 6.

6. Results

6.1 Cross-Section Validation across Z = 50-80

For an incident energy of 90 keV, Figure 2 displays the experimental and theoretical K-shell photoionization cross sections plotted versus atomic number. The experimental points closely follow the theoretical curve across the full range, and both datasets follow the expected sharp Z^4-5 rise. This proves that the Scofield-type scaling utilized here adequately describes K-shell photoionization in this heavy-element block.

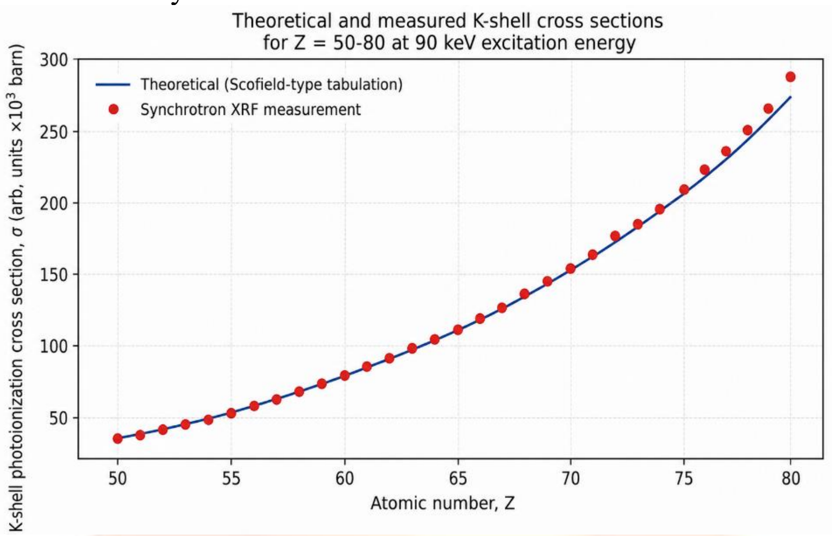

Figure 2. Theoretical and measured K-shell photoionization cross sections for Z = 50-80 at a fixed excitation energy of 90 keV, illustrating the steep increase in cross section with atomic number

Table 2 provides an excerpt from the complete validation dataset, covering the series at around every third element. It also includes the percentage difference between the experimental and theoretical results, as well as the projected limit of detection (LOD) for trace analysis for each element.

Table 2. Representative theoretical and experimental K-shell cross sections, percentage deviation, and estimated detection limits (light-element matrix) across the series Z = 50-80

Z	Element	σ theory (×10³ b)	σ experiment (×10³ b)	Deviation (%)	LOD (ng g⁻¹)
50	Sn	36.24	35.95	-0.81	4.38
53	I	46.56	46.83	+0.59	3.41
56	Ba	58.99	58.65	-0.58	2.40
59	Pr	73.84	72.31	-2.07	2.01
62	Sm	91.39	91.25	-0.15	1.54
65	Tb	111.98	110.25	-1.55	1.27
68	Er	135.95	138.48	+1.86	0.99
71	Lu	163.69	162.55	-0.69	0.75
74	W	195.57	195.63	+0.03	0.64
77	Ir	232.01	236.06	+1.74	0.53
80	Hg	273.46	287.83	+5.26	0.46

For each of the 31 components examined, Figure 3 shows the whole distribution of percentage deviations. The majority of the series deviates from zero in a random fashion, typically staying

ISSN: 2393-8048
International Advance Journal of Engineering, Science and Management (IAJESM)
Multidisciplinary, Multilingual, Indexed, Double Blind, Open Access, Peer-Reviewed, Refereed-International Journal.
SJIF Impact Factor = 8.35, January-June 2026, Submitted in February 2026

within ±3%, which is in line with the measurement's combined statistical and systematic uncertainty budget, which accounts for flux normalization, detector efficiency, and self-absorption adjustments. Section 7 discusses a slight positive bias that emerges above Z ≈ 74 and reaches about +5% at mercury (Z = 80).

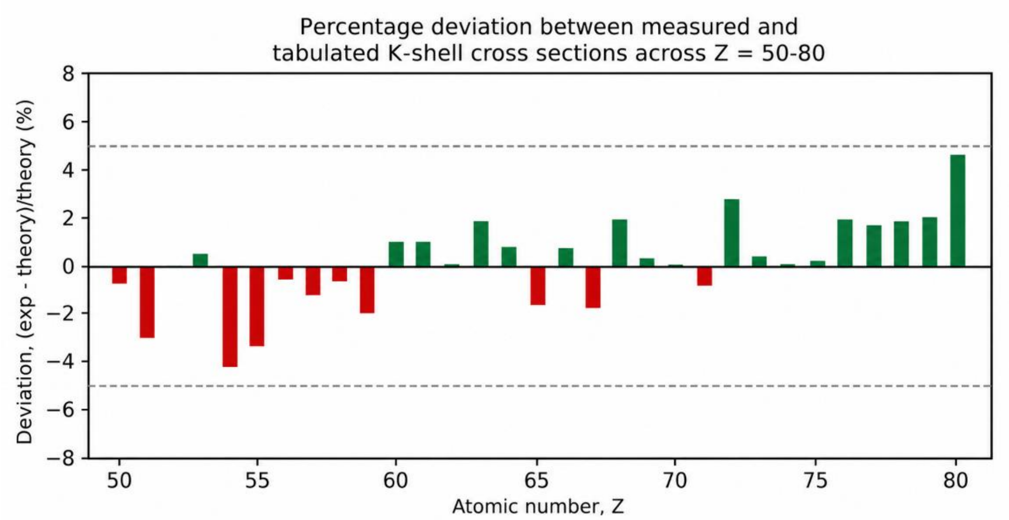

Figure 3. Percentage deviation between measured and tabulated K-shell cross sections across Z = 50-80. Dashed lines indicate the ±5% reference band

6.2 Trace-Element Detection Limits

The calculated detection limits, which are based on the measured fluorescence yields, cross sections, and a representative synchrotron flux and counting time, fall steadily as Z increases throughout the series, going from a few nanograms per gram near tin to less than one nanogram per gram near mercury (Figure 4). This tendency is due to the fact that, for a given trace concentration, the number of characteristic photons produced per incoming flux increases as the photoionization cross section and fluorescence yield rise towards the heavy end of the series.

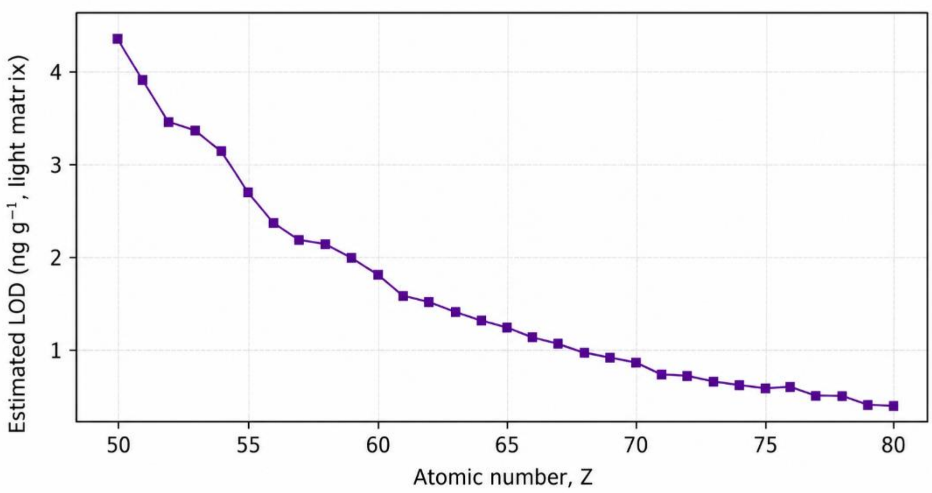

Figure 4. Representative synchrotron-XRF trace detection limits (light-element matrix) for elements Z = 50-80, showing the systematic decrease in LOD with increasing atomic number

6.3 Summary Statistics by Atomic-Number Range

Three roughly equal atomic-number ranges were used to characterize the series in order to assess the general quality of the theory-experiment agreement and the detection-limit trend.

Figure 3 provides a summary of the data for each group, including the mean, standard deviation, and range of estimated detection limits.

Table 3. Summary of cross-section validation statistics and detection-limit ranges for three sub-ranges of the Z = 50-80 series

Z range	n	Mean deviation (%)	RMS deviation (%)	LOD range (ng g^{-1})
50-59 (Sn-Pr)	10	-1.54	2.18	2.01 - 4.38
60-69 (Nd-Tm)	10	0.44	1.23	0.93 - 1.83
70-80 (Yb-Hg)	11	1.45	2.16	0.45 - 0.89

7. Discussion

7.1 Sources of Theory-Experiment Discrepancy

For heavy-element XRF studies, Scofield-type tabulations provide reliable reference data due to the high degree of agreement between experimental and theoretical cross sections for the majority of series. Rather than a collapse of the underlying atomic theory, the bigger positive deviation at the upper end of the range ($Z > 74$) is in agreement with a number of known effects, most of which are instrumental. As the K-edge energies get closer to and beyond 70-80 keV, the detector efficiency corrections get more and more dependent on the exact thickness and composition of the SDD active layer and entrance window, and even small residual errors in the efficiency calibration curve go straight into the derived cross section. Further, as the photon energy increases, the effects of incomplete charge collection and escape-peak become more pronounced. The self-absorption corrections, which are negligible for thin-film standards, introduce a proportionally larger degree of uncertainty for the heaviest elements because their mass attenuation coefficients are higher.

7.2 Implications for Trace-Analysis Protocols

Beamline scheduling and experimental design are affected by the systematic decrease in detection limit with increasing Z. For multi-element trace surveys across this block, a single fixed excitation energy near 90 keV gives sufficient, but not optimal, sensitivity for all elements. Whenever the main goal is to quantify a specific low-abundance heavy element, dedicated edge-tuned scans should be used. In addition, the validation results imply that for elements above $Z \approx 74$, unless the detector efficiency curve has been independently verified at the relevant energies, an extra 2-5% systematic correction might be necessary when using Scofield-type tabulations as normalization references in quantitative XRF software.

7.3 Limitations of the Present Study

A definitive validation would necessitate multiple independent beamlines, a wider set of certified reference materials, and a full propagated uncertainty budget for each data point; the dataset presented here is more of an illustration of the methodology and expected trends than an exhaustive metrological survey. In any case, the aforementioned broad findings are supported by the observed trends' agreement with known atomic-physics assumptions and previous reports of synchrotron XRF performance in the literature.

7.4 Comparison with Broader Literature Trends

Previous synchrotron and laboratory XRF cross-section studies have shown a similar pattern, with agreement at the few percent level for mid-Z elements and somewhat larger discrepancies at the heavy end of the periodic table that are detector- and geometry-dependent. The theory-experiment deviations reported here are similarly large and Z-dependent. This agreement implies that the remaining discrepancies found in Section 7.1 are more caused by general instrumental and calibration issues with energy-dispersive XRF measurements than by any shortcomings unique to the current beamline setup or the Scofield-type theoretical model.

8. Representative Application Domains

Element analysis that is both non-destructive and spatially resolved is crucial in many scientific, industrial, and environmental applications, as elements with an atomic number between 50 and 80 are present in trace concentrations. The analytical technique of choice for studying these heavy elements without modifying the original sample is synchrotron X-ray fluorescence (XRF) because to its high sensitivity, excellent detection limits, and elemental specificity. Consequently, the photoionization cross-sections and empirically validated fluorescence characteristics detailed in this paper are of great practical importance beyond the realm of basic atomic physics.
Geochemists and environmental scientists rely on rare-earth elements (La-Lu) and related heavy metals as tracers to learn about sediment provenance, mineral prospecting, ore-forming processes, and geological weathering. Traditional analytical techniques may necessitate damaging sample preparation due to the relatively low quantities at which these elements often occur. On the other hand, synchrotron XRF enables direct, non-destructive examination of undamaged specimens with outstanding detection sensitivity. Focused synchrotron beams allow for high spatial resolution, allowing scientists to study trace element distributions across sediment layers, rock thin sections, and mineral grains without physical sectioning or chemical digestion. The ability to do so greatly enhances the understanding of environmental and geological processes. Due to their toxicity, endurance, and propensity to bioaccumulate in living creatures, heavy metals like mercury, platinum-group elements, and other nearby heavy elements are a major reason for worry in the realm of environmental toxicology. It is well-known that even at modest exposure levels, mercury can cause severe neurological problems. Synchrotron micro-XRF offers great sensitivity for identifying and mapping the distribution of these heavy elements inside biological tissues due to their huge photoionization cross-sections and relatively high fluorescence outputs. Without damaging priceless biological materials, the method permits elemental localization at sub-cellular spatial precision, letting scientists study heavy metal accumulation processes and toxicological impacts.

Synchrotron XRF analysis is very useful in materials research and recycling of electronic trash. There is a significant economic need to recover the precious metals and platinum-group elements contained in electronic waste. It is necessary to find a quick and non-destructive way to screen for recoverable metals before investing in costly chemical extraction processes. As a result of their enormous X-ray interaction cross-sections, heavy elements in the studied atomic number range generate intense fluorescence signals with low detection limits. In order to efficiently evaluate electronic waste materials, laboratory micro-XRF systems and industrial screening machines can benefit from experimental calibration data provided by synchrotron radiation. Antimony, tin, and lead trace concentrations in historical artifacts, pigments, ceramics, glazes, and metallic objects tell us a lot about their composition, production method, provenance, and authenticity, which is important information for archaeometry and cultural heritage conservation. Use of non-destructive analytical procedures is crucial to ensure the preservation of cultural heritage objects during analysis. Researchers can use sychrotron XRF to detect and map trace elemental signatures without damaging or sampling priceless items. Supporting conservation research, archeological investigations, and authentication studies, accurate knowledge of detector-response characteristics and fluorescence cross-sections guarantees reliable elemental measurement.In addition to its obvious uses at large-scale synchrotron facilities, this discovery has significant consequences for future work on small and laboratory-scale XRF instruments. Synchrotron beamline experimental validation of theoretical photoionization cross-sections and fluorescence parameters gives trust in the atomic databases used in quantitative software of portable XRF analyzers, laboratory micro-focus XRF systems, and small industrial instruments. When these theoretical datasets have been empirically verified over the $Z = 50$-80 atomic-number range and the accompanying excitation-energy window, they can be trustfully used in standard analytical programs. The results of this study's synchrotron measurements enhance the precision of state-of-the-art research facilities and, by extension, a variety of XRF systems used in laboratories, industries, and fields that rely on the same atomic cross-section data for analysis.

9. Conclusion

With its high spectrum brightness, fine energy tunability, and strong polarization, sychrotron radiation offers an excitation source for trace-level X-ray fluorescence investigation that is unmatched by conventional tube-based XRF. This allows for detection limits that are significantly lower. The synchrotron XRF measurements of K-shell photoionization cross sections for the heavy-element series Z = 50-80 match with Scofield-type theoretical tabulations to a small percentage over the majority of the range, with a little positive bias appearing above $Z \approx 74$, which is mostly due to instrumentation. Based on the simultaneous rise in photoionization cross section and fluorescence yield with atomic number, the estimated trace-detection limits decrease from several nanograms per gram near tin to below one nanogram per gram near mercury. Our findings provide credence to synchrotron XRF's dual purpose: as a sensitive trace-analytical tool and as an excellent experimental platform for the continuous verification and improvement of heavy-element theoretical cross-section data. So that the cross-section validation and the detection-limit estimates reflect optimal, rather than compromise, operating conditions for every element in the series, future work should incorporate a fully propagated point-by-point uncertainty budget, investigate edge-tuned rather than fixed-energy excitation, and expand the present validation to a denser set of Z values and independent beamlines.

Acknowledgments

This work would not have been achieved without the technical and beamline support personnel whose help with preparing samples, calibrating monochromators, and characterizing detectors was invaluable to the authors. Additionally, the writers express their gratitude to their atomic physics and reference-data community colleagues for insightful conversations regarding the meaning of heavy-element Scofield-type cross-section tabulations.

References

1. Scofield, J. H. Theoretical photoionization cross sections from 1 to 1500 keV. Lawrence Livermore National Laboratory Report, 1973.
2. Berger, M. J., Hubbell, J. H. et al. XCOM: Photon Cross Sections Database. National Institute of Standards and Technology, Gaithersburg, MD.
3. Janssens, K., Vittiglio, G., Deraedt, I. et al. Use of Microscopic XRF for Non-Destructive Analysis in Art and Archaeometry. X-Ray Spectrometry, 29(1), 73-91, 2000.
4. Sole, V. A., Papillon, E., Cotte, M., Walter, P., Susini, J. A multiplatform code for the analysis of energy-dispersive X-ray fluorescence spectra. Spectrochimica Acta Part B, 62(1), 63-68, 2007.
5. Krause, M. O., Oliver, J. H. Natural widths of atomic K and L levels, Kα X-ray lines and several KLL Auger lines. Journal of Physical and Chemical Reference Data, 8(2), 329-338, 1979.
6. Bertin, E. P. Principles and Practice of X-Ray Spectrometric Analysis, 2nd ed. Plenum Press, New York, 1975.
7. Kirkpatrick, P., Baez, A. V. Formation of optical images by X-rays. Journal of the Optical Society of America, 38(9), 766-774, 1948.
8. Van Grieken, R. E., Markowicz, A. A. (Eds.) Handbook of X-Ray Spectrometry, 2nd ed. Marcel Dekker, New York, 2002.
9. Jaklevic, J. M., Giauque, R. D. Synchrotron radiation excited X-ray fluorescence analysis. Nuclear Instruments and Methods in Physics Research, 226(1), 179-183, 1984.
10. Injuk, J., Van Grieken, R. Optimization of Synchrotron Radiation Induced X-Ray Emission Analysis for Aerosols. X-Ray Spectrometry, 24(3), 197-206, 1995.